Doping effects on the ferroelectric transition of multiferroic Y(Mn,Al/Ga)O_3

Hasung Sim,[1,2] Haeri Kim,[1,2] Kisoo Park,[1,2] Martin Lilienblum,[3] Manfred Fiebig,[3] and Je-Geun Park[1,2,*]

[1]*Center for Correlated Electron Systems, Institute for Basic Science, Seoul 08826, Korea*

[2]*Department of Physics & Astronomy, Seoul National University, Seoul 08826, Korea*

[3]*Department of Materials, ETH Zurich, 8093 Zurich, Switzerland*

(Received 13 February 2018; revised manuscript received 7 July 2018; published 20 August 2018)

Multiferroic hexagonal manganites $RMnO_3$ have a very high ferroelectric transition temperature around and above 1200 K, depending on the rare-earth elements, and a reasonably large electric polarization of about 5.5 $\mu C/cm^2$ at room temperature. It is generally believed that the ferroelectric transition is driven by the combination of R-O_P displacement and MnO_5 tilting, and hence called improper ferroelectric. In order to better understand the improper ferroelectric transition, we studied doping effects, using two elements with the same valence but a different ionic size: Al and Ga on the Mn site of $YMnO_3$. Through detailed structural studies and nanoscale measurements of piezoresponse force microscopy (PFM) we conclude that there is a drastic doping effect for Al, whose ionic size is much smaller than Mn. It is in stark contrast with our observation that Ga, having a slightly smaller ionic size with Mn, does not change the ferroelectric transition up to 50% doping. This drastic difference in the doping effect is due to local strain induced by the difference in the ionic size of Al and Mn as compared with that of Mn, and sheds light on the intriguing nature of the improper ferroelectric transition.

DOI: 10.1103/PhysRevB.98.085132

I. INTRODUCTION

Hexagonal manganite, in particular $YMnO_3$, is one of the popular multiferroic materials with a ferroelectric transition around $T_C \sim 1200$ K and an antiferromagnetic transition around $T_N \sim 75$ K [1]. The ferroelectric transition of hexagonal manganites is driven by a strong trimerization structural transition and so called improper [2,3]. Naturally the cross coupling of the magnetic moment and the electric polarization have been under intensive studies: although a linear magnetoelectric effect [4] is forbidden by the symmetry, a nonlinear coupling between magnetic moment and polarization is, in principle, possible. It is now well understood that the hexagonal manganites host an unusually large spin-lattice coupling as seen in various experiments such as diffraction [5], Raman spectroscopy [6–8], and IR spectroscopy [9,10]. More recently, it was shown that this spin-lattice coupling produces hybrid magnon-phonon excitations, which were observed by inelastic neutron scattering experiments [11]. The aspect that makes hexagonal manganites unique is that it has a two-dimensional triangular lattice with a MnO_5 polyhedral network. This leads to geometrical frustration effects in magnetism.

The hexagonal manganites $RMnO_3$ (R = Sc, Y, In, Dy-Lu) undergo a structure transition from a paraelectric $P6_3/mmc$ (No. 194) to a ferroelectric $P6_3cm$ (No. 185) structure. Note that for the $P6_3cm$ structure Mn sits at the 6c position of (x o z) and we refined the data with $z = 0$. Though there are papers reporting an intermediate phase in between [12,13], we found that it is a rather abrupt, close to a weak first-order transition with no intermediate phase [14]. In principle, a total of four separate modes, namely Γ_1^+, Γ_2^-, K_1, and K_3, are activated during the transition [15]. Among the four modes, the K_3 mode that triples the cell is a primary order, which itself can be separated into two components: a R-O_P displacement mode that includes the c direction movements of R and O_P ions, which are antiferroelectric, and a MnO_5 tilt mode. According to the latest high-temperature structure studies, the R-O_P displacement appears to be the primary order parameter of the phase transition with almost first-order character [14]. This R-O_P displacement is then accompanied by MnO_5 tilting and a Γ_2^- polarization mode.

Doping studies on the hexagonal manganites so far were mostly concentrated on the magnetism side. (We want to mention that as both Al and Ga have the same valence as Mn, the main effect of doping here is the chemical pressure effect and so local strain.) For example, it was found that with increasing doping concentration on the Mn site the signatures of the antiferromagnetic ordering get subdued. On the other hand, doping at the rare-earth site seems to have much weaker effects: the antiferromagnetic transition seems to remain unchanged across the whole doping range of (Y, Lu)MnO_3 [16]. Enhancement of magnetoelectric coupling [17] and thermal conductivity [18] at the magnetic transition were also reported for Ga-doped $YMnO_3$ in addition to the structural studies on the Ga-doped samples at room temperature [19]. Although experimental works are scarce on the doping effects on the ferroelectric transition, a theoretical study found that Ga doping on $InMnO_3$ induces a change in the space group as the doping ratio increases [20]. Given the lack of experimental studies on the doping effects on the ferroelectric transition and their change of ferroelectric to a nonpolar state, it is an interesting question how the ferroelectric transition responds

*jgpark10@snu.ac.kr

to controlled perturbations via doping at the Mn site. It will be especially useful if one can follow the temperature and doping dependence in detail of those key distortion modes, in particular K_3 with the R-O_P displacement mode and the MnO_5 tilt mode, found in the pure system.

In this paper we report the extensive studies of Al and Ga doping at the Mn site. The ionic radius of Al^{3+} is 0.675 Å, whereas Ga^{3+} has an ionic radius of 0.76 Å, slightly smaller than that of Mn^{3+} (0.785 Å). We should also comment that while $YGaO_3$ was reported to be ferroelectric with the same hexagonal structure, $YAlO_3$ is paraelectric with an orthorhombic structure [21,22]. We aimed to explore how the variations in the ionic size affect the ferroelectric transition. In doing so, we hoped that it would reveal hitherto unknown doping effects on the ferroelectric transition. To examine the high-temperature structural changes carefully, we employed both x-ray powder-, and single-crystal diffraction (XRD) techniques. In addition, we used a piezoresponse force microscopy (PFM) to probe the ferroelectricity directly. In this study, we found that as the Al-doping ratio increases, the ferroelectricity is rapidly suppressed and the transition temperature decreases. In contrast, there is surprisingly very little doping effect when we used Ga up to 50%. We discuss these results in terms of local strain effects on the ferroelectric transition.

II. EXPERIMENTAL DETAILS

We prepared polycrystalline $YMn_{1-x}(Al/Ga)_xO_3$ using Y_2O_3, Mn_2O_3, and Al_2O_3/Ga_2O_3 by a standard solid-state reaction method. All the starting materials were prepared in stoichiometric ratio and mixed, pelletized, and sintered several times. The final sintering condition was set to 1300 °C for 24 h. Single crystals were subsequently grown with a 4-mm-diameter feed rod of correct composition by a floating-zone furnace (Crystal Systems, Japan) under ambient conditions at a growth speed of 2 mm/h. We note that while the usual solid-state reaction method can only yield up to 10% doping [23], our single-crystal growth can produce samples with much higher doping: 50% in the case of Ga doping. We also succeeded in growing single crystals of $YMn_{1-x}Al_xO_3$ up to $x = 0.25$. All our samples were checked to form in the single phase by powder and single-crystal XRD measurements.

We performed high-temperature powder XRD experiments from 300 to 1473 K using a commercial diffractometer (D8 Advance, Bruker) after grinding the grown single crystals into fine powder. We also carried out single-crystal XRD using a high-resolution single-crystal x-ray diffractometer (XtaLAB P200, Rigaku) from 300 to 1073 K, employing a gas flow type heater. We refined all our data using FullProf [24].

Afterwards, we made PFM measurements using an atomic force microscope system (Asylum Cypher, Oxford Instruments). Pt/Ir-coated Si cantilevers (NCH/Pt, resonance frequency: 350 kHz, Nanoworld) were used for both PFM measurements. PFM images were acquired by applying an ac modulation voltage of 10 V and a frequency of 350 kHz to the tip before and after applied biases over a square-shaped region of 1 μm × 1 μm (−10 V) and 3 μm × 3 μm (+10 V). Prior to the SPM experiments, the samples were heated to 150 °C for 30 min to remove water molecules that might have been unintentionally adsorbed on the surface.

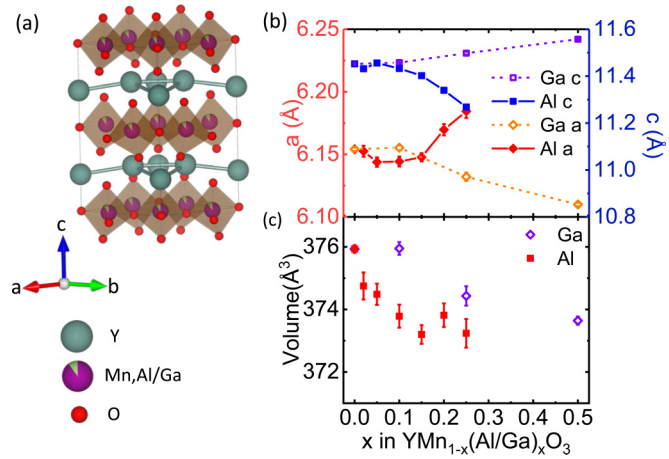

FIG. 1. (a) Structure of $YMn_{1-x}(Al/Ga)_xO_3$, (b) lattice constant, and (c) unit-cell volume as a function of doping ratio.

III. RESULTS AND ANALYSIS

$YMnO_3$ has the $P6_3cm$ structure at room temperature. According to our XRD results, all our samples yield the same space group $P6_3cm$ regardless of the Al- or Ga-doping concentration. Figure 1(a) shows the crystal structure of $YMn_{1-x}(Al/Ga)_xO_3$. Figures 1(b) and 1(c) show the lattice constants and volume as a function of Al and Ga doping, measured by single-crystal XRD. As one can see, there is a gradual change in the lattice constant as the doping ratio increases. Note that Al and Ga doping have an opposite effect. While Al doping increases the a lattice constant and decreases the c lattice constant, Ga doping produces the exactly opposite effects. But the overall qualitative effect on the unit-cell volume is the same as both Al and Ga have smaller ionic size than Mn: ionic radius is Mn^{3+}(78.5 pm) > Ga^{3+}(76 pm) > Al^{3+}(67.5 pm). Thus, it is interesting to ask how Ga and Al, having smaller ionic size, have such completely opposite effects on the a and c lattice constants. As we will argue, it is likely related to the doping dependence on Y-O hybridization and the ferroelectric transition.

In order to study the doping dependence on the ferroelectric transition directly, first we collected high-resolution XRD data at room temperature. Figure 2 shows the powder XRD data for all Al- and Ga-doping values, which confirm that there are no impurity peaks for all the samples. As compared with earlier works by Ismailzedt *et al.* [25], we found that the hexagonal phase can be stabilized up to higher Al concentration in our case as we have grown our single crystal using a floating zone technique. Although there have been some discussions [1,26,27], it is now generally accepted that $YMnO_3$ undergoes a structural and improper ferroelectric transition from the $P6_3/mmc$ structure to the $P6_3cm$ structure at 1250 K, at which several new superlattice peaks appear [14]. Among the superlattice peaks present below the transition, we marked a few strong peaks in Figs. 2(a) and 2(c): they are the (102), (104), (204), and (212) peaks. We also plotted the (212) peak separately to further highlight the doping dependence of its intensity. As clearly seen in the figures, the superlattice peaks get suppressed progressively with Al doping and seem to disappear for higher than 15% of Al doping. In contrast, the

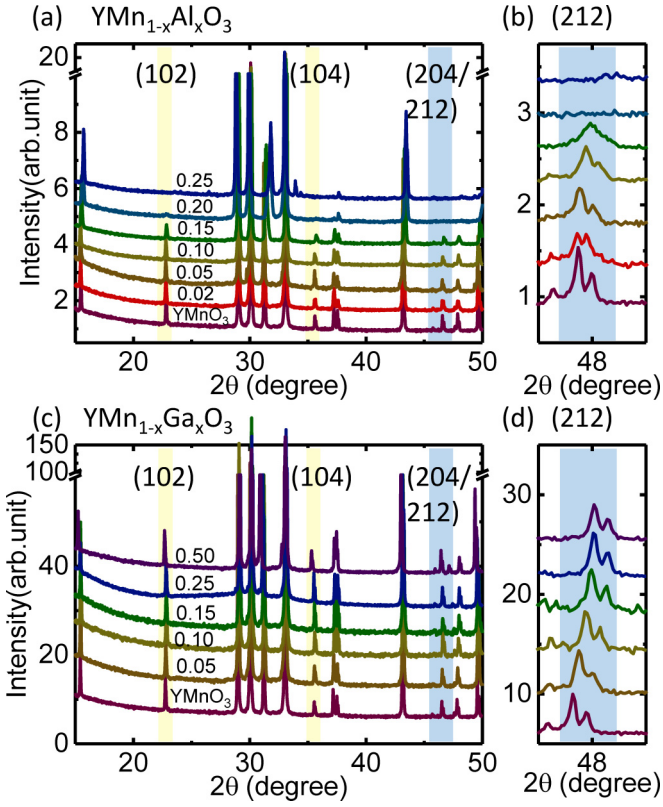

FIG. 2. Powder XRD results of (a) $YMn_{1-x}Al_xO_3$ and (c) $YMn_{1-x}Ga_xO_3$. The highlighted region represents the main superlattice peaks that are directly related to the structural transition. (b) and (d) The enlarged picture of the (212) peaks for $YMn_{1-x}Al_xO_3$ and $YMn_{1-x}Ga_xO_3$, respectively.

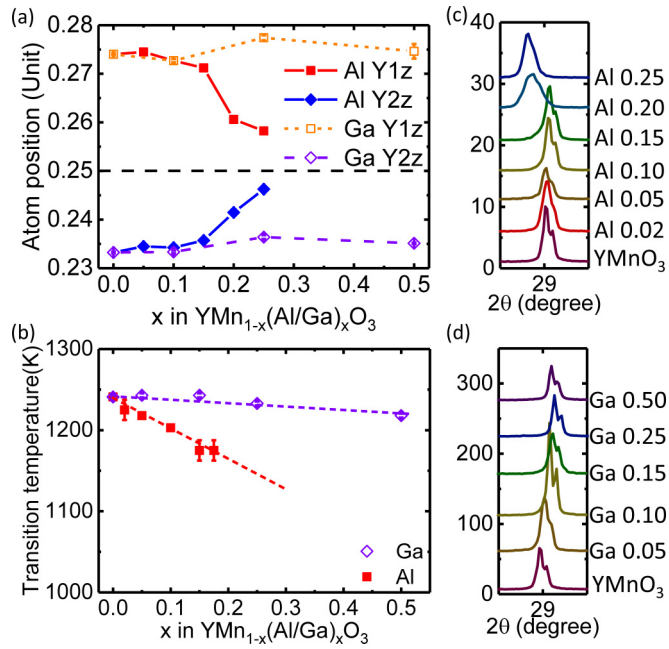

FIG. 3. (a) Refinement results of the z position of Y from single crystal XRD data. (b) Ferroelectric transition temperature as a function of Al/Ga doping ratio. $Y1$ and $Y2$ are at the 2a and 4b positions of $P6_3cm$, respectively. (c) and (d) The doping dependence of the (1 1 0) peaks for Al and Ga doping with significant peak broadening observed for those Al-doped samples.

same superlattice peaks remain unchanged even up to 50% of Ga doping. This strikingly different doping dependence on the superlattice peaks indicates that both Al and Ga with smaller ionic size produce completely different effects on the ferroelectric transition.

Figure 3(a) shows the Y atomic position at room temperature as a function of doping, which was determined from the single-crystal XRD data. As one can see, with Al doping the Y position converges to the value of 0.25, indicating that it comes closer to the structure of the paraelectric $P6_3/mmc$ phase with an ideal triangular lattice of Mn atoms. On the other hand, the Y position remains almost unchanged with Ga doping, again supporting our conclusion that the ferroelectric phase is still robust for the Ga-doped samples almost as strong as in the pure sample. We obtained the full transition-temperature phase diagram using data collected from two XRD machines (powder and single crystal). Note that since the intensity of the superlattice peaks get significantly decreased with increasing temperature, especially near the transition temperature, we used both powder and single-crystal XRD machines to plot the data points in Fig. 3(b). The transition temperature was greatly reduced when the Al doping ratio was increased, whereas it remained nearly unchanged with the Ga doping even up to 50%.

In order to check this doping dependence on the ferroelectric transition temperature, we have carried out high-temperature powder XRD studies with some representative data shown in Fig. 4. As summarized in the temperature dependence of the (212) peak, there are noticeable differences in the doping effects. First, with Al doping the transition temperature is reduced quite significantly from 1250 K for the pure sample to 1175 K for the 15% of Al doping. Second, the transition that is originally a weak first order for the pure sample [14] becomes very smooth for the 15% doping, indicating that it has become a second-order transition for the doped samples. The lines underneath the data points are our fitting results using Ginzburg-Landau free energy with a weak first order for pure, 5%, and 10% doping and a second order for 15% doping. On the other hand, there is little noticeable effect on the overall temperature dependence for all the Ga-doped samples. We note that somewhat large increase in T_c was reported in Ref. [18] although we do not know at the moment what causes the difference as compared with our data. Our data exhibit neither a change in the transition temperature nor in the nature of the transition. This result may be due to the reported transition temperature of $YGaO_3$, 1020 K, not being much different from that of $YMnO_3$ (1250 K) [22]. All the lines drawn for the Ga-doped samples are for a weak first order. To make this point clearer, we show an enlarged picture of the data near the transition temperature as an inset.

To further confirm the ferroelectric property of the doped $YMnO_3$, we compared the piezoresponse pre- and post-application of a bias voltage through the PFM experiments. We note that our PFM measurements were done at room temperature. Figures 5(a)–5(c) show the results for pure $YMnO_3$, $YMn_{0.9}Al_{0.1}O_3$, and $YMn_{0.75}Ga_{0.25}O_3$. For example,

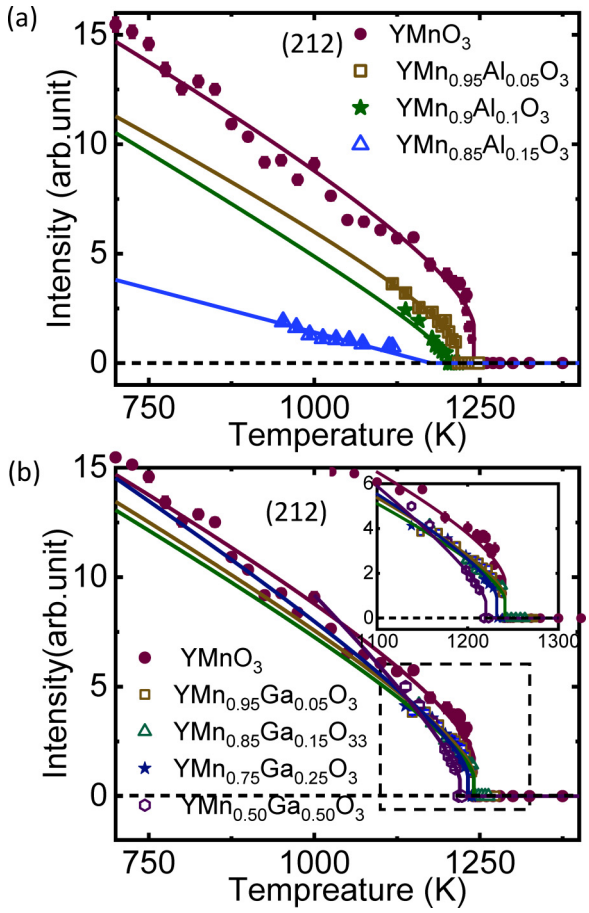

FIG. 4. Temperature dependence of the (212) peaks due to the R-O_P displacement mode: (a) Al and (b) Ga doping. The solid lines represent our Ginzburg-Landau analysis with a first-order transition for all the samples, except for $YMn_{0.85}Al_{0.15}O_3$ (blue line), for which we used a second-order model. Inset in (b) shows the enlarged picture of the data near the transition temperature marked by the dashed line in the main figure. All the data were collected on powder samples that were prepared by crushing the single-crystal samples.

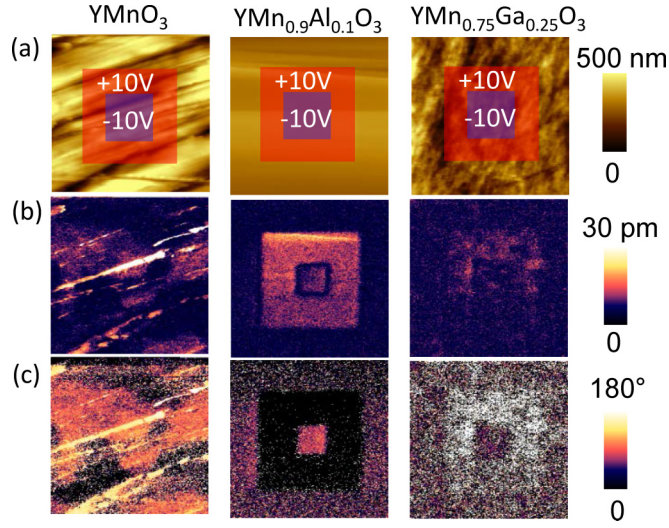

FIG. 5. (a) AFM images. (b) and (c) PFM amplitude and phase signal, of three samples: $YMnO_3$ (first column), $YMn_{0.9}Al_{0.1}O_3$ (second column), and $YMn_{0.75}Ga_{0.25}O_3$ (third column) after applied bias over a square-shaped region of 1 μm × 1 μm (−10 V, overlaid with blue) and 3 μm × 3 μm (+10 V, overlaid with red) at the central region.

the pure sample displays distinct ferroelectric domains [28], which are consistent with the fact that it is harder to switch the ferroelectric domain of the undoped sample. On the other hand, our 10% Al-doped sample shows a clear sign of poling: our XRD data found that Al doping reduces the transition temperature and changes its character to more like a second-order transition. In any case, our data suggest that Al doping significantly reduces the coercive field. By comparison, the 25% Ga-doped sample shows more or less similar behavior to those of the undoped sample. Overall, our PFM data are consistent with the conclusion drawn from the diffraction data that up to 10% of Al and 25% of Ga doping the samples still remain ferroelectric.

IV. DISCUSSION AND SUMMARY

When we discuss the doping effects of Al and Ga, a first factor to be considered is that both Al and Ga disrupt the Mn network. If this should be the main factor for the ferroelectric transition of doped samples, then we would anticipate seeing similar effects for both Al and Ga doping. However, the fact that we witnessed completely opposite doping effects on the transition temperature strongly indicate that the disruption of the Mn network is not the leading factor. It is a very surprising result if one is reminded that the MnO_5 titling was originally proposed as triggering the ferroelectric transition [2]. Thus, our observation seems to contradict the original proposal and instead calls for a better explanation. A second factor worth considering is the chemical pressure effects. But we can also discard it based on the experimental observation that at 50% Ga doping the unit-cell volume is about the same at the 25% of Al doping. Thus, if the chemical volume effect is the sole major factor, then again we cannot explain why our 50% Ga-doped sample is still ferroelectric while our 25% Al-doped sample yields a considerably weaker ferroelectric transition or no transition at all.

These considerations require us to look for other explanations for the experimental results. For this, we note that although Al and Ga have smaller ionic size than Mn, the ionic size of Ga is relatively closer to that of Mn. It basically means that there is a much larger, *local*, strain field generated around the Al-doping site than what is expected for Ga doping at the same doping level, or for the same unit-cell volume. We found that all the Bragg peaks get broadened with Al doping, which is in sharp contrast with those of Ga doping with very little change in the width [see Figs. 3(c) and 3(d)]. This significant broadening only seen in the Al-doped samples is a clear sign that Al doping induces stronger, local strain effects as expected of the larger difference in the ionic radius with respect of that of Mn. Generally, strain is known to have direct but, sometimes, mixed effects on a ferroelectric transition. As mentioned, the R-O_P displacement mode is a primary order parameter, which is then accompanied by the MnO_5 tilting and the Γ_2^- polarization mode in $YMnO_3$. What is interesting about

our data is that local strain induced by doping with different ionic sizes seems to be coupled to the R-O_P displacement primary order parameter of the improper ferroelectricity of $YMnO_3$, changing greatly the nature of the order parameter as demonstrated by the temperature dependence of our XRD data. Eventually, it would affect the Γ_2^- mode, which governs the ferroelectricity of $YMnO_3$. This indirect coupling between local strain and the ferroelectricity is rather unusual and unique.

As a further comment, we can think of several implications of our work on the issues related to the hexagonal manganites. First and foremost, the change in the nature of the ferroelectric transition seen in Fig. 4 has an important consequence on the domain physics. The intriguing domains found in hexagonal manganites were interpreted in terms of the Kibble-Zurek mechanism [29]. As the transition undergoes some kind of qualitative change with Al and Ga doping, it is an interesting question how this doping-induced change in the nature of the ferroelectric transition affects the domain patterns. Second, as the Al-doped samples seem to require a smaller switching voltage it may be easier to realize the ME coupling that has so far been proven more difficult for the hexagonal manganites. Third, with the lower switching voltage it may be found more useful for future development of FeRAM.

To summarize, we investigated how Al and Ga doping at the Mn sites of $YMnO_3$ affects the improper ferroelectric transition by using powder and single-crystal diffraction techniques together with PFM measurements. By combining all the data, we conclude that the ferroelectric transition is disproportionately suppressed by Al doping and nearly destroyed by more than 15% of Al doping. In contrast, the ferroelectric transition remains unaffected by Ga doping up to 50%. We think that these strikingly different doping effects are due to local strains induced by doping and the improper nature of the ferroelectricity of $YMnO_3$.

ACKNOWLEDGMENTS

We would thank Y. Noda, D. Khomskii, and N. Spaldin for useful discussions. We should also acknowledge the valuable comments made by the anonymous referees, which were helpful for us to improve the paper. This work was supported by Institute for Basic Science (IBS-R009-G1).

[1] H. Sim, J. Oh, J. Jeong, M. D. Le, and J.-G. Park, Acta Crystallogr. Sect. B **72**, 3 (2016).
[2] B. B. Van Aken, T. T. M. Palstra, A. Filippetti, and N. A. Spaldin, Nat. Mater. **3**, 164 (2004).
[3] S-W. Cheong and M. Mostovoy, Nat. Mater. **6**, 13 (2007).
[4] M. Fiebig, T. Lottermoser, D. Meier, and M. Trassin, Nat. Rev. Mater. **1**, 16046 (2016).
[5] S. Lee, A. Pirogov, M. Kang, K-H. Jang, M. Yonemura, T. Kamiyama, S.-W. Cheong, F. Gozzo, N. Shin, H. Kimura, Y. Noda, and J.-G. Park, Nature (London) **451**, 805 (2008).
[6] C. Toulouse, J. Liu, Y. Gallais, M.-A. Measson, A. Sacuto, M. Cazayous, L. Chaix, V. Simonet, S. de Brion, L. Pinsard-Godart, F. Willaert, J. B. Brubach, P. Roy, and S. Petit, Phys. Rev. B **89**, 094415 (2014).
[7] A. P. Litvinchuk, M. N. Iliev, V. N. Popov, and M. M. Gospodinov, J. Phys.: Condens. Matter **16**, 809 (2004).
[8] J. Vermette, S. Jandl, A. A. Mukhin, V. Y. Ivanov, A. Balbashov, M. M. Gospodinov, and L. Pinsard-Gaudart, J. Phys.: Condens. Matter **22**, 356002 (2010).
[9] M. Zaghrioui, V. Ta Phuoc, R. A. Souza, and M. Gervais, Phys. Rev. B **78**, 184305 (2008).
[10] R. Basistyy, T. N. Stanislavchuk, A. A. Sirenko, A. P. Litvinchuk, M. Kotelyanskii, G. L. Carr, N. Lee, X. Wang, and S.-W. Cheong, Phys. Rev. B **90**, 024307 (2014).
[11] J. Oh, M. D. Le, H.-H. Nahm, H. Sim, J. Jeong, T. G. Perring, H. Woo, K. Nakajima, S. Ohira-Kawamura, Z. Yamani, Y. Yoshida, H. Eisaki, S.-W. Cheong, A. L. Chernyshev, and J.-G. Park, Nat. Commun. **7**, 13146 (2016).
[12] C. J. Fennie and K. M. Rabe, Phys. Rev. B **72**, 100103(R) (2005).
[13] J. Kim, Y. M. Koo, K.-S. Sohn, and N. Shin, Appl. Phys. Lett. **97**, 092902 (2010).
[14] H. Sim, J. Jeong, H. Kim, S.-W. Cheong, and J.-G. Park, J. Phys.: Condens. Matter **30**, 105601 (2018).
[15] T. Lonkai, D. G. Tomuta, U. Amann, J. Ihringer, R. W. A. Hendrikx, D. M. Tobbens, and J. A. Mydosh, Phys. Rev. B **69**, 134108 (2004).
[16] S. Choi, H. Sim, S. Kang, K-Y Choi, and J.-G. Park, J. Phys.: Condens. Matter **29**, 095602 (2017).
[17] A. A. Nugroho, N. Bellido, U. Adem, G. Nénert, Ch. Simon, M. O. Tjia, M. Mostovoy, and T. T. M. Palstra, Phys. Rev. B **75**, 174435 (2007).
[18] H. D. Zhou, J. C. Denyszyn, and J. B. Goodenough, Phys. Rev. B **72**, 224401 (2005).
[19] U. Adem, A. A. Nugroho, A. Meetsma, and T. T. M. Palstra, Phys. Rev. B **75**, 014108 (2007).
[20] S. M. Griffin, M. Reidulff, S. M. Selbach, and N. A. Spaldin, Chem. Mater. **29**, 2425 (2017).
[21] R. Diehl and G. Brandt, Mater. Res. Bull. **10**, 85 (1975)
[22] S. C. Abrahams, Acta Crystallogr. Sect. B **57**, 485 (2001).
[23] J. Park, M. Kang, J. Kim, S. Lee, K.-H. Jang, A. Pirogov, J.-G. Park, C. Lee, S.-H. Park, and H. C. Kim, Phys. Rev. B **79**, 064417 (2009).
[24] J. Rodriguez-Carvajal, Physica B **192**, 55 (1993).
[25] I. H. Ismailzad, G. A. Smolensk, V. I. Nesterenk, and F. A. Agaev, Phys. Status Solidi **5**, 83 (1971).
[26] A. S. Gibbs, K. S. Knight, and P. Lightfoot, Phys. Rev. B **83**, 094111 (2011).
[27] M. Lilienblum, T. Lottermoser, S. Manz, S. M. Selbach, A. Cano, and M. Fiebig, Nat. Phys. **11**, 1070 (2015).
[28] K. Kobayashi, H. Kamo, K. Kurushima, Y. Horibe, S.-W. Cheong, Y. Togawa, and S. Mori, J. Kor. Phys. Soc. **62**, 1077 (2013).
[29] S-Z. Lin, X. Wang, Y. Kamiya, G-W. Chern, F. Fan, D. Fan, B. Casas, Y. Liu, V. Kiryukhin, W. H. Zurek, C. D. Batista, and S-W. Cheong, Nat. Phys. **10**, 970 (2014).